DEFENCE R&D DÉFENSE

# Response of HF Radar to Meteor Backscatter Detection

T. Thayaparan
*Defence Research Establishment Ottawa*

DEFENCE RESEARCH ESTABLISHMENT OTTAWA

TECHNICAL REPORT
DREO TR 1999-100
October 1999

National Defence Défense nationale

Canada

101-02523/

DEFENCE R&D DÉFENSE

# Response of HF Radar to Meteor Backscatter Detection

T. Thayaparan
*Ground Based Radar Group*
*Surface Radar Section*

**DEFENCE RESEARCH ESTABLISHMENT OTTAWA**

TECHNICAL REPORT
DREO TR 1999-100
October 1999

Project
05AB11

## Abstract

The response of High Frequency (HF) and Very High Frequency (VHF) radar systems to echoes from underdense meteor trails is numerically calculated. A comparison is made at radar frequencies of 5, 15, 25, and 40 MHz based on standard echo theory. This theory takes account of the initial radius of the trail, the finite formation due to the meteor velocity, and the diffusion in the time between radar sweeps. Height distributions of underdense meteor echoes are predicted based on standard theory as a function of radar frequency. The importance of data processing scheme is highlighted in order to detect underdense meteor echoes at different radar frequencies. The strengths and drawbacks for radar detection of meteors at a low frequency are discussed.

## Résumé

La réponse des systémes radars à ondes décamétrique et à trés haute fréquence aux échos des traces de météores à faible densité est calculée numériquement. Une comparaison est faite à partir de la théorie des échos standard pour les fréquences radar de 5, 15, 35, et 40 MHz. Cette théorie tient compte du rayon initial des traces, de la formation finie due a la vitesse des météores, et la diffusion dans le temps entre chaque balayage radar. La hauteur des distributions des échos météores à faible densité est prédis à partir de la théorie standard en fonction de la fréquence radar. L'importance des méthodes de traitement de données est accentuer en vue de détecté des échos de météores à faible densité à différente fréquence radar. Les avantages et problémes de la détection des météores aux basses fréquences sont discutés.

## Executive Summary

One of the ionospheric clutters that degrade the detection capability of aircraft and missile targets by High Frequency (HF) radar is meteors. The performance of HF radars is at times adversely affected by meteors while receiving radar signal. Although sophisticated signal processing techniques have been developed to minimize the interference from meteors, the effectiveness of these techniques is highly dependent on the characteristics of meteor clutter. *Chan* [1998] demonstrated that meteor echoes can degrade the High Frequency Surface Wave Radar's (HFSWR) aircraft detection performance by masking the echoes of aircraft targets having similar Doppler shifts. In addition, he showed that meteor echoes can cause excessive false alarms because the spectral characteristics of meteor echoes are very similar to those of a manoeuvring target. Therefore, our understanding of the meteor behaviour is required in order to optimize the detection performance of the HF radar. As such, this report contributes additional insight, which may aid in developing a better algorithm to identify and remove meteors from the signal.

This report will concentrate on the numerical analysis to the responses of High Frequency (HF) and Very High Frequency (VHF) radar systems to echoes from underdense meteor trails. A comparison is made at different radar frequencies of 5, 15, 25, and 40 MHz based on standard echo theory. This theory takes account of the initial radius of the trail, the finite formation due to the meteor velocity, and the diffusion in the time between radar sweeps. Height distributions of underdense meteor echoes are predicted based on the standard theory as a function of radar frequency. The importance of data processing scheme is highlighted in order to detect underdense meteor echoes at different radar frequencies. The advantages and drawbacks are discussed for radar detection of meteors at low frequencies.

Author, Thayaparan, Thayananthan, Response of HF radar to meteor backscatter detection, Defence Research Establishment Ottawa, DREO TR 1999-100, November 1999.

## Sommaire

Les météores sont un des fouillis ionosphériques qui diminue la capacité de détection des radars décamétrique à ondes de surface (RDOS) contre des avions et des missiles. La performance des RDOS est quelquefois affectée négativement par des météores pendant la réception des signaux radars. Des techniques sophistiquées de traitement de signaux ont été développées pour réduire au maximum les interférences des météores. Cependant, l'efficacité de ces techniques est grandement dépendante des caractéristiques du fouillis météores. *Chan* [1998] a démontré que les échos météores peuvent dégrader la performance de détection des avions en masquant les échos des cibles par des déplacements Doppler similaire. De plus, Il a montré que les échos météores sont très similaires à ceux des avions effectuant des manoeuvres. Par conséquent, une compréhension du comportement des météores est nécessaire en vue d'optimiser la performance de détection des RDOS. Ainsi, ce rapport fournit une contribution additionnelle qui peut aider a développer de meilleurs algorithmes pour identifier et enlever le fouillis météore des signaux.

Ce rapport se concentre sur l'analyse numérique des réponses des systémes radars à ondes décamétrique et à trés haute fréquence aux échos des traces de météores à faible densité. Une comparaison est faite à partir de la théorie des échos standard pour les fréquences radar de 5, 15, 35, et 40 MHz. Cette théorie tient compte du rayon initial des traces, de la formation finie due à la vitesse des météores, et la diffusion dans le temps entre chaque balayage radar. La hauteur des distributions des échos météores à faible densité est prédis à partir de la théorie standard en fonction de la fréquence radar. L'importance des méthodes de traitement de données est accentuer en vue de détecté des échos de météores à faible densité à différente fréquence radar. Les avantages et problémes de la détection des météores aux basses fréquences sont discutés.



Auteur, Thayaparan, Thayananthan, Réponse des radars décamétrique à ondes de surface aux détection des échos météores, Centre de Recherches pour la Défense, Ottawa, DREO TR 1999-100, Novembre 1999.

# Table of Contents


Abstract/Résumé iii

Executive Summary v

Sommaire vi

List of Figures ix

1 Introduction 1
1.1 What is a Meteor ? . . . 1
1.2 Sporadic and Shower Meteors . . . 1
1.2.1 The Dangers of Meteor Showers . . . 3
1.3 The Formation of the Ionized Column . . . 4
1.4 Underdense and Overdense Meteor Trails . . . 5
1.5 Specular Reflection . . . 6
1.6 Daily and Monthly Variation of Meteor Rates . . . 6
1.7 Radar Measurements . . . 7

2 Radar Detection of Meteors 8
2.1 Ambipolar Diffusion . . . 9
2.1.1 Importance of PRF . . . 13
2.1.2 Wind-induced effects . . . 14
2.2 Initial Radius of the Trail . . . 17
2.3 Finite Meteor Velocity . . . 20
2.4 Total Attenuation . . . 22
2.5 Sampling Time Interval . . . 24

3 Radio wave backscattering from an underdense meteor trail 25

4 Height Distribution of Meteors 30

5 Radar Detection of Meteors at Low Frequency 32

6 Conclusion 35

# List of Figures


1 Logarithmic ambipolar diffusion coefficient plotted as a function height. . . . 11

2 Logarithmic decay time constant plotted as a function height and frequency 12

3 The height distribution of the amplitude attenuation factor, $\alpha_d$, due to diffusion for four different radar frequencies at PRF=100 Hz. . . . . 13

4 Contours of zonal mean winds in $ms^{-1}$ at latitudes for 40° N and 50° N. . . 15

5 The height distribution of initial radius, $r_0$, for three different velocities. . . . 18

6 The height distribution of the amplitude attenuation factor, $\alpha_r$, due to initial radius effect for three different velocities. . . . . 19

7 The height distribution of the amplitude attenuation factor, $\alpha_V$, due to finite velocity effect for three different velocities. . . . . 20

8 The height distribution of $\alpha_V$ as a function of range, $R$, for a radar frequency of 25 MHz and velocity of 40 m/s. . . . . 21

9 Amplitude attenuation factors at $f = 5$ MHz radar frequency. The values of the four $\alpha's$ are plotted as functions of height at three velocities (20, 40, 60 km/s). The pulse repetition frequency used is 100 Hz. The range used in the computation is $R = 300$ km. . . . . 22

10 As for Figure 6 except $f = 15$ MHz. . . . . 23

11 As for Figure 6 except $f = 25$ MHz. . . . . 24

12 As for Figure 6 except $f = 40$ MHz. . . . . 25

13 The geometry of the meteor path relative to the observing station. . . . . 26

14 Height distributions of underdense meteor trails at radar frequencies of 5, 15, 25, and 40 MHz. . . . . 31

# 1 Introduction

## 1.1 What is a Meteor ?

The word "meteor" is derived from the Greek "Meteoros" meaning "things up in the air" or "raised beyond". A meteor is a bright streak (meteor trail) across the night sky resulting from the heat generated when a particle or piece of matter travelling at a high velocity in space enters the Earth's atmosphere. The particle itself is called a meteor, but it is preferable to designate it as a meteoroid [*McKinley,* 1961]. A meteoroid then produces a meteor when it encounters and interacts with the Earth's atmosphere. A very bright meteor is called a fireball, and a large fireball, particularly one accompanied by sparks and a explosive noise, is called a bolide. While most meteoroids will disintegrate into small particles and dust upon entering our atmosphere, some of the very largest will make an impact with the surface of the Earth creating large craters [*Hawkins,* 1964].

## 1.2 Sporadic and Shower Meteors

There are two main types of meteors: sporadic and shower meteors. Sporadic meteors may be seen on almost any night of the year at the rate of 1 to 7 per hour and show no preferred direction in the sky. The greatest sporadic meteors occurs after, rather than before, midnight. Between midnight and dawn an observer is facing the same direction as the Earth is moving in its orbit and as such he can see all of the meteors formed by the meteoroids travelling towards him. On the other hand, between dusk and midnight, the only meteors that are visible are those produced by meteoroids coming towards him with sufficient velocity to overtake the Earth [*Lovell,* 1954; *McKinley,* 1961].

The other type of meteor that occurs is the meteor shower. Meteor showers are regular appearances of enhanced meteor flux, which occur at the same time every year, and appear to be coming from the same direction (known as a radiant) [*McKinley,* 1961]. Meteor showers take their names from the constellation or star near where their radiant position is located. Most meteor showers occur regularly each year, some meteor showers occur every few years, and a few meteor showers occur only once every few decades. Many meteor showers can be predicted, as they repeat every year when the Earth passes through the path of a comet.

Every year the Earth experience about a dozen major meteor showers. For example, every August we experience the Perseids, every December we have the Geminids, and every November we have the Leonid meteor shower. What this means is that, if one goes out and looks at the dark sky on any given night, one will see 1 to 7 meteors ("shooting stars") per hour. If one does that each year on November 17, one will see 10 to 15 meteors per hour, in other words the Leonid meteor shower. Meteor showers are the result of the encounter between the Earth and the debris left behind by comets. Comets are thought to be large agglomerations of ice with bits and pieces of rock and dust which are interspersed throughout. Comets are formed in the cold outer reaches of the solar system. When, for some reason the orbits are perturbed, they come into the inner solar system, and in some cases, take paths which cross the orbit of the Earth. As the comet approaches the Sun, it begins to heat up, and the ice boils off, taking with it the rock and dust. This solid material follows roughly the same path as the comet. Hence, when the Earth later passes through the same region of space that the comet previously passed through, we encounter the debris cloud. The entry of the small pieces of rock into the Earth's atmosphere at high speeds causes them to burn up and in the process produce a flash of light. The flash of light is the meteor we see from the Earth's surface [*Hawkins,* 1964].

In the past three years, the Leonid meteor shower has received a great deal of attention in the media. In November of each year, the Earth passes through the debris cloud from comet Tempel-Tuttle. This event generally creates a meteor shower as the dust enters the Earth's atmosphere and burns up. Since the debris appears to be coming from the direction of the constellation Leo, the meteor shower is called the "Leonid shower". The meteor flux associated with the Leonid shower is normally about 10 to 15 per hour. In 1998, 1999, and 2000, the Earth is in the process of passing very close to the comet's orbital path at a time when the comet has recently passed by. As such scientists predict 200 to 5000 meteors per hour or possibly more than that of the characteristic for a normal year of 10 to 15 meteors per hour [*Yeomans,* 1996]. Meteor detection rates for previous apparitions of the Leonid shower are given by *Jenniskens* [1995] for 1866, 1867, 1966, and 1969. An exceptionally high peak rate of 150,000 meteors per hour was observed in 1966, the most intense shower on record, although Jenniskens also notes that this rate may be in error and that the actual rate might have been around 15,000. Using historical accounts of the Leonid showers from AD 902 to 1933, *Newton* [1864] established a time of 33.25 years between major shower events. Further description of this subject is beyond the scope of this report.

### 1.2.1 The Dangers of Meteor Showers

The particles from a cometary debris cloud are typically very small, smaller than the diameter of a human hair, and tend to burn up at very high altitudes. None reach the surface of the Earth and there is no danger to the Earth's surface or to any aircraft.

However in space, we have a different story. Our satellites are not protected by the atmosphere. Although the particles of rock and dust are very small, the encounter velocity is enormous, about 72 km/second (or even 155,000 miles per hour, over 200 times the speed of sound). The result being that even a grain of sand the size a pin head is equivalent to the energy of a 0.22 caliber bullet [*McDonnell et al.*, 1997].

At these high speeds, even a tiny particle can cause sensitive damage to the electronic components or induce electrical problems. While major holes and physical damage to solar panels and structures are very unlikely, impacts of small particles will create an electrically charged plasma (a plasma is a cloud of mixed positive and negative charges) which can induce electrical shorts and failures in sensitive electronic components. All satellites both military and civilian at all orbital altitudes are at risk from this natural disaster.

Concern has been expressed over the effects of the Leonid meteor shower on the man-made satellites orbiting Earth. There are over 500 active satellites now in orbit above the Earth, and they will be sandblasted during the passage through the cometary debris. Given that we know now, the intensity of the Leonid shower in 1998 or 1999 is lower than it was in 1966. Thus, it is unlikely that a large number of satellites will be "knocked out".

It is possible that some satellites will be damaged, but the most likely sources of damage will not be from a rock "blasting a hole" in a satellite, but rather, from the creation of a plasma, or free electric charge on the spacecraft. The charge could cause damage to computers and other sensitive electronic circuits on board the spacecraft, and ultimately cause the spacecraft to malfunction. For example, during the 1993 Perseid shower, it was determined that Olympus communications satellite was damaged by a meteor strike and went off the air shortly thereafter as a result of an electrical failure [*Caswell et al.*, 1995].

## 1.3 The Formation of the Ionized Column

Meteor trails are formed by the ablation of particles whose initial mass lies between the range $10^{-8}$ to tens of grams, orbiting the Sun either in individual paths (sporadic meteors) or as members of streams with a common orbit (shower meteors). When a meteoroid encounters air molecules in the upper atmosphere, the surface temperature of the impinging particle increases until fusion and vaporization begins. Evaporated meteoric atoms then collide with other air molecules, ionizing them and resulting in a neutral column of positive ions and electrons. Therefore, a meteor trail is a column of ionized particles. For radar purposes a trail is characterized by its maximum ionization line density $q$ electrons/meter. The general expression of $q$ is given by:

$$q = \frac{\tau_q \Lambda A}{4 \zeta \eta} \left(\frac{m}{\rho_m}\right)^{2/3} \rho_a V^4 \tag{1}$$

where $m$ is the meteoroid mass, $\rho_m$ is the meteoroid density, $\rho_a$ is the air density, $V$ is the meteoroid velocity, $A$ is the shape factor of the meteoroid, $\Lambda$ is the heat transfer coefficient, $\zeta$ is the heat of ablation of the meteoroid material, $\eta$ is the mean ionization potential of the ionized atoms, and $\tau_q$ is the ionization efficiency factor. A more detailed discussion of the parameters involved in equation (1) is given by *McKinley* [1961] and *Hughes* [1978].

For underdense trail (see the following section) it has been established that the maximum ionization line density is proportional to the mass and velocity of the meteoroid, and the empirical formula is given by:

$$q = 7.7 \times 10^{-10} m^{0.92} V^{3.91} \tag{2}$$

where $q$ is the ionization line density in $\mathrm{m}^{-1}$, $m$ is the meteoroid initial mass in grams, and $V$ is the meteoroid velocity in $\mathrm{cm\,s}^{-1}$. As an example, the value $q = 10^{10}\ \mathrm{m}^{-1}$ corresponds to a meteoroid mass of about $10^{-6}$ g when the velocity is $V = 35\ \mathrm{km\,s}^{-1}$. Note that expressions (1) and (2) can be valid only for particles with the ability to produce ionization.

Once a column of electrons has been produced in the wake of the passage of the meteoroid, it forms an effective reflector to MF, HF and VHF electromagnetic radiation. All radio techniques applied in this field of study depend on the scattering of incident electromagnetic

waves from the ionized matter in a meteor trail, and the free electrons in the plasma are important elements in the scattering process.

## 1.4 Underdense and Overdense Meteor Trails

Two distinct regimes exist in the detection of meteor trails by radar, these being the so-called underdense and overdense conditions. In the underdense regime the radio wave penetrates the trail with little attenuation and each electron acts as an independent scatterer. The echo from such a trail is characterized by a rapid initial rise in echo strength, followed by small amplitude fluctuations due to diffraction effects during the formation of the trail [e.g., *Davies and Ellyett,* 1949]. In an overdense trail the electron density is sufficiently high such that the radio wave does not penetrate the trail, but is reflected by the trail as a whole. This overdense trail behaves more like a macroscopic conducting surface or a small scale ionosphere [e.g., *Greenhow,* 1952]. These echoes may also show the rapid initial rise in amplitude, followed by diffraction fluctuations. In contrast to underdense trail, the amplitudes remains fairly constant for some time and then rapidly fall to zero. It is usual to express the electron density as a line density, that is, the number of electrons per unit length of the trail. The transition from the underdense to the overdense condition occurs at $q = 2.4 \times 10^{14}$ electrons per meter [*Kaiser et al.,* 1969; *Bronsthen,* 1983]. It is largely independent of the radio wavelength (for a detailed discussion of the above, see *McKinley* [1961]).

*Booker* [1956] showed that meteor trails at a mean height of 95 km reflecting 8 m wavelength waves for more than 0.4 s could be considered as overdense. Overdense echoes can be identified from echo duration exceeding 0.4 s and from the irregular fading of the echo amplitude produced by the interference between the discrete echoes received simultaneously from different parts of the trail with different Doppler frequency shifts. Recently, *Jones and Jones,* [1990] showed that the trails can transgress from overdense to underdense due to dilution of the ionized cloud from reactions of that cloud with ozone (for trails near 80 km height).

For most radars the number of echoes from underdense trails greatly exceeds those from overdense trails, and the proportion increases with increasing radar sensitivity. Echoes from underdense trails are referred to as 'decay-type' echoes (see below) due to ambipolar diffusion and/or recombination and attachment, dependent upon the individual meteor's height.

## 1.5 Specular Reflection

The radio echo from a meteor trail at the wavelengths used in drift studies (e.g., 20-50 MHz radar frequency) is essentially of the diffraction type, where destructive interference reduces the returns from most parts of the trail so that only the first Fresnel zonal contributes effectively to the echo. In meteor studies the size of the first Fresnel zone is usually of the order of 1 km ($\approx 2(\frac{R\lambda}{2})^{\frac{1}{2}}$, where $R$ is the range and $\lambda$ is the radar wavelength), and the specular reflection point on a meteor is generally located within this zone [*McKinley,* 1961]. The specular reflection point (for a station or pair of stations) is the point on the trail at minimum distance from the station, or minimum sum of distances from a pair of stations [*Grossi et al.,* 1972]. That is, detection of a meteor echo requires that some point on the trail should be intersected by a perpendicular from the radar station and that the trail should be included in the central Fresnal zone as seen from the radar. The requirement perpendicularity means that the radar response is dependent not only on the position of the trail within the radar beam, but is also strongly dependent on the trail orientation. The process of detecting meteor trails with backscatter radar (as in our case) is a specular one, with the majority of the reflected energy coming from the first Fresnel zone about the specular reflection point. However, for overdense trails the radar echo lasts long enough to be deformed by wind shears, producing more than one specular reflection [*Booker,* 1956].

## 1.6 Daily and Monthly Variation of Meteor Rates

If no appreciable shower activity is present, the rate of meteors will vary from a minimum around 1800 hours local time to a maximum in the early morning hours around 0600. Normally the daily high-low ratio will be in the range 3 to 5. The observed diurnal variation is the result of the relative motion between the Earth and the meteors recorded by the radar [e.g., *Whipple,* 1954; *Lovell,* 1954]. The morning maximum and evening minimum are a natural consequence of the Earth's motion in its orbit. Because the Earth is moving in its orbit $\sim$ 30 km/s, we will encounter more meteors when we are on the "forward side" of the Earth at around 0600 local hours, than we will 12 hours later. The late afternoon meteors will have to catch up with the Earth. Hence there will be fewer of them and their resultant velocities will be lower [e.g., *McKinley,* 1961]. The recognized meteor shower, of course, can markedly affect the normal diurnal distributions. For example, when January Quadrantids occur in the late afternoon, the total number of meteors per hour may well exceed the rates

recorded the following morning when the sharp peak of the shower has passed. Similarly, the daytime showers of May to July elevate the midday rates for several weeks each year.

The monthly variation of the meteor rate is the result of the sporadic radiant sources, namely apex, helion, antihelion, and toroidal sources, changing their strengths significantly during the year [e.g., *Stohl,* 1968; *Mawrey and Broadhurst,* 1993; *Jones and Brown,* 1994]; this leads to non-uniform spatial density of meteors along the Earth's orbit. In general, the observed monthly variation shows that the rate of meteors will vary from a minimum around spring to a maximum around Fall in the northern hemisphere [e.g., *McKinley,* 1961; *Avery et al.,* 1983]. The apex of the earth's way is above the horizon of an observer in the northern hemisphere for more hours each day during September than it is during March. One would thus expect that the monthly rates in the northern hemisphere would show a maximum around September and a minimum around March. On the other hand, in the Southern hemisphere the apex is highest in March and lowest in September, so that the natural expectation is that the monthly rates would be greatest around March and least around September.

## 1.7 Radar Measurements

The upper atmosphere of the Earth is continuously being bombarded by meteoroids which, on encountering the increasing density of the atmosphere produce (if large enough) visible light and a trail of ionization. Typical sizes might be anything from as small as a grain of dusts or larger. Generally meteors enter the atmosphere at velocities of $\sim$ 12-72 km/s and quickly vaporize at heights between 80 and 100 km, forming long columns of ionized particles. Appleton had suspected in his early observations of the ionosphere, that the sudden appearance of some type of ionization around the E-region is due to meteors [e.g., *Appleton and Barnett,* 1925]. Meteors had been studied by radio methods for astronomical interests before 1960. The meteor trail movement became a subject of study for observing winds at meteor heights in the 1950s [e.g., *McKinley and Millman,* 1949; *Manning et al.,* 1953]. Since then radar observations of meteors have been carried out for the past 50 years. Much is known about the nature and origin of meteoroid bodies and of the process of ablation in the Earth's upper atmosphere, which produces a trail of ionization detectable by radio reflection. Most radio observations of meteors have been made along line-of-sight paths and at radar frequencies above about 20 MHz for which ionospheric effects are largely absent.

Recent years have seen the development of large HF sky wave radars for long range defence

and surveillance purposes [*Anderson*, 1986; *Chan*, 1998]. As a by-product of their primary defensive role, such radar systems possess excellent sensitivity for the detection of meteor echoes. Such meteor echoes can be used to calibrate the radar system and to estimate other parameters. The measurement of the echo duration of radio meteors is important in several fields of study. Since the reflection process of radio waves from meteor trails is predominantly specular for underdense meteors, the duration of the echo contains important information about altitude and elevation of the meteor echo.

More recently meteor echoes have also been used to determine temperature fluctuations at meteor heights [e.g., *Hocking et al.*, 1997]. Although meteors can be used in several fields of study, this report will concentrate on the response of a HF radar to meteors. In the following sections we confine ourselves to echoes backscattered from underdense trails.

# 2 Radar Detection of Meteors

The ability of the meteor radar to detect underdense meteor trails depends on many factors. If the radius of the ionized column is comparable with or larger than $\frac{\lambda}{2\pi}$ ($\lambda$ = operating radar wavelength) then the radiation backscattered from electrons in the near and far sides of the trail will not be in phase, and these reflected wave components will interfere destructively. The resultant echo will therefore be severely attenuated [e.g., *Manning*, 1958; *Poulter and Baggaley*, 1977, 1978]. A long wavelength radar is therefore immediately seen to be preferable. However, there are many drawbacks such as: (1) the size of the antenna array necessary to achieve a high gain; (2) broadcast and natural interference; (3) ionospheric absorption; and (4) confusion with ionospheric echoes. Because of these reasons conventional meteor radars have normally been operated at wavelengths of around 5-15 m.

The factors which determine the strength of the amplitude of a radar echo from an underdense meteor trail during the formation and initial evolution of that trail have been reviewed (amongst others) by *Greenhow and Hall* [1955], *Greenhow and Neufeld* [1955], *Greenhow and Hall* [1960], *McKinley* [1961], *Olsson-Steel and Elford* [1987], *Thomas et al.* [1988], and *Steel and Elford* [1991]. The main factors which cause the attenuation in echo amplitude are (1) ambipolar diffusion, (2) the initial radius of the trail, and (3) the finite meteor velocity effect. The attenuation factors given throughout this section are those describing the attenuation in amplitude rather than in power.

## 2.1 Ambipolar Diffusion

One of the main factors which causes the attenuation in echo amplitude is ambipolar diffusion. As a meteoroid ablates in the Earth's atmosphere the evaporated atoms are ionized in the collisions with air molecules resulting in the formation of a plasma trail, i.e., the trail of ions and electrons, which is able to scatter radio waves. If a radio wave impinges on such trails at an angle normal to the trail, then a portion of the wave energy is scattered back along the direction from which it has come.

After the trail has formed, it begins to dissipate by, among other processes, ambipolar diffusion, eddy diffusion, turbulence, recombination, and chemical reactions. Diffusion dominates for a few seconds while turbulence is the chief mechanism for trails lasting 30 s or more [e.g., *Thomas et al.*, 1988]. Diffusion causes the column to expand radially and when it is illuminated by radio waves the degree of interference of contributions to the scattered wave from different parts of the cross-section of the train determine the amplitude of the radio-meteor echo. It is generally true that ambipolar diffusion is the dominant factor in the early stages of trail growth, and therefore primarily determines the echo intensity for underdense trails near meteor heights [e.g., *Jones*, 1975]. It can be shown that the backscattered amplitude from an underdense trail decreases exponentially with time due to ambipolar diffusion in the manner:

$$A = A_0 \exp(\frac{-t}{\tau_d}) \tag{3}$$

where $A_0$ is the initial amplitude at $t$=0 (typically the time at which the exponential decay begins) and $A$ is the amplitude after time $t$. The echo decay time constant $\tau_d$ is given by:

$$\tau_d = \frac{\lambda^2}{16\pi^2 D_a} \tag{4}$$

which defines the duration to $1/e$ of the initial amplitude [e.g., *Kaiser*, 1953; *McDaniel and Mason*, 1973]. Note that $\tau_d$ depends only upon the wavelength $\lambda$ and ambipolar diffusion coefficient $D_a$. Thus at a given $\lambda$ and $D_a$ the echoes from all underdense trails decay with the same time constant. Echoes from underdense trails are therefore referred to as 'decay-type-echoes' [*Phillips*, 1969].

Decay times ($\tau_d$) have been used in several studies to investigate temporal variability of the ambipolar diffusion coefficient $D_a$ [e.g., *Tsutsumi et al.*, 1994; *Reddi et al.*, 1993; *Chilson et al.*, 1996]. However, recent theory has shown that $D_a$ is proportional to $T^2/P$, where $T$ is a temperature and $P$ is a pressure, so if either $T$ or $P$ is known, the other parameter can be deduced [e.g., *Jones and Jones*, 1990; *Jones*, 1995]. In this work, we present neither $T$ nor $P$ but rather $D_a$ and discuss its usefulness for the detection capabilities.

Next we examine how the properties of the neutral atmosphere and the charged ions affect $D_a$. To begin we consider a dilute system of ions and electrons in a neutral gas. Although in isolation each component of a plasma would diffuse at its characteristic rate, when together they diffuse at the same rate since any tendency for one component to diffuse more rapidly is suppressed by a space charge field. It can be shown that if we neglect electron-ion collisions,

$$D_a = D_i (1 + \frac{T_e}{T_i}) \tag{5}$$

where $D_i$ is the ionic diffusion coefficient, and $T_e$ and $T_i$ are the electron and ion temperatures, respectively [*Kaiser*, 1953; *Bittencourt*, 1986]. It is common to assume that the ions and electrons rapidly reach thermal equilibrium with the neutral gas through collisional processes. *Jones* [1975] support the assumption for heights up to 100 km but this is not necessarily so in meteor trails above 100 km. For such a case:

$$D_a \approx 2\, D_i \tag{6}$$

For the case of a vanishing electric field, the ionic diffusion coefficient $D_i$ is given through the Einstein relation as:

$$D_i = \frac{k\,T}{q_e} (\frac{T}{273.16}) (\frac{1.013 \times 10^5}{P})\, K_0 \tag{7}$$

where $k$ is the Boltzmann constant, $q_e$ is the electronic charge ($= 1.6 \times 10^{-19}$ C), and $T$ and $P$ are the temperature and pressure of the neutral gas, respectively [*McDaniel and Mason*, 1973]. $K_0$ is a constant related to the nature of the plasma in the trail. If metallic ions ($M^+$) are the main ionic constituent and $N_2$ is the main neutral species, then $K_0 = 2.5 \times 10^{-4} m^2 s^{-1} V^{-1}$. It should be noted that this is an "average" value represen-

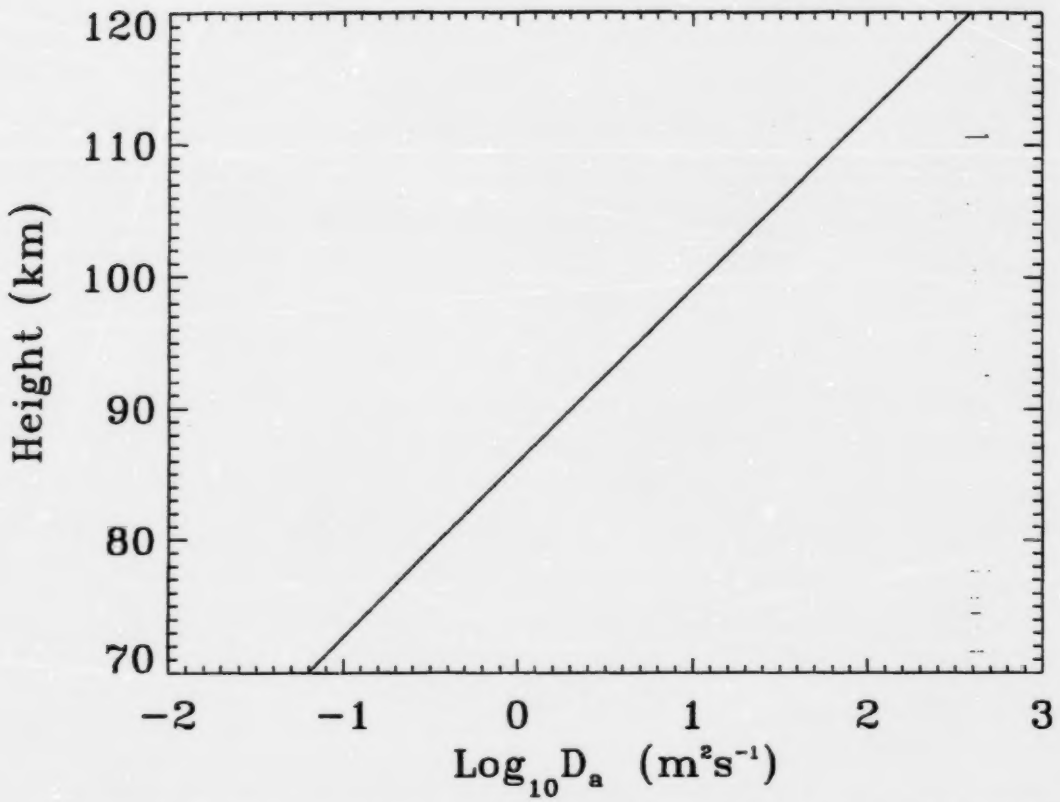


Figure 1: Logarithmic ambipolar diffusion coefficient plotted as a function height.

tative of ions having mass numbers between those of $Mg^+$ and $Fe^+$. If $N_2^+$ is the main ion, $K_0 = 1.9 \times 10^{-4} m^2 s^{-1} V^{-1}$ [e.g., *Chilson et al.*, 1996; *Jones and Jones*, 1990; *Jones*, 1995]. *Chilson et al.* [1996] found that they should use the latter value of $K_0$. We have adopted the more usual assumption that the main ions are $M^+$ (i.e., $K_0 = 2.5 \times 10^{-4}$). Equations (6) and (7) can be used in equation (4) to predict the decay rates of meteor trail echoes.

Using the U.S. Standard Atmosphere $D_a$ is approximated over the height range 80-125 km by [*Thomas et al.*, 1988]:

$$\log_{10} D_a = 0.0758\, h - 6.51 \qquad (8)$$

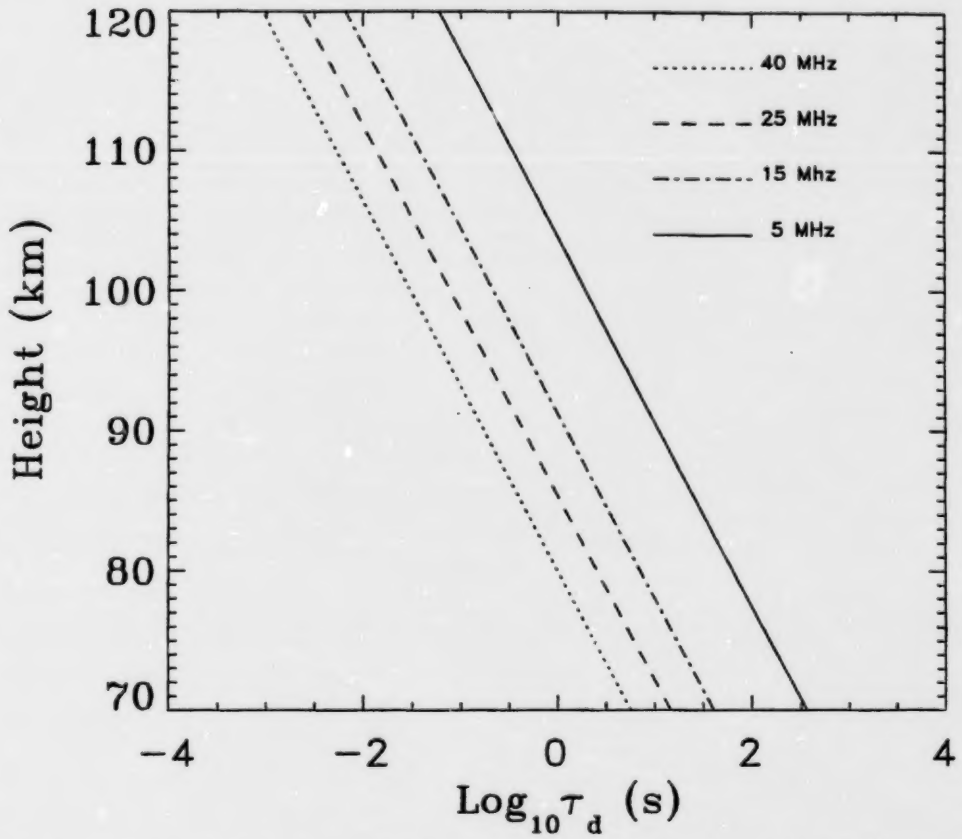


Figure 2: Logarithmic decay time constant plotted as a function height and frequency

Figure 1 illustrates the ambipolar diffusion coefficient $D_a$ as a function of height. It should be noted that, on occasions, larger temperature gradients are found in the meteor region and the relationship between $\log_{10} D_a$ and $h$ is then no longer linear. Figure 2 illustrates the decay time constant $\tau_d$ as a function of height and frequency.

### 2.1.1 Importance of PRF

It is important to note that if the pulse repetition frequency (PRF), i.e., the number of pulses per second, of the radar is low, then it is possible that fast-decaying echoes are less likely to

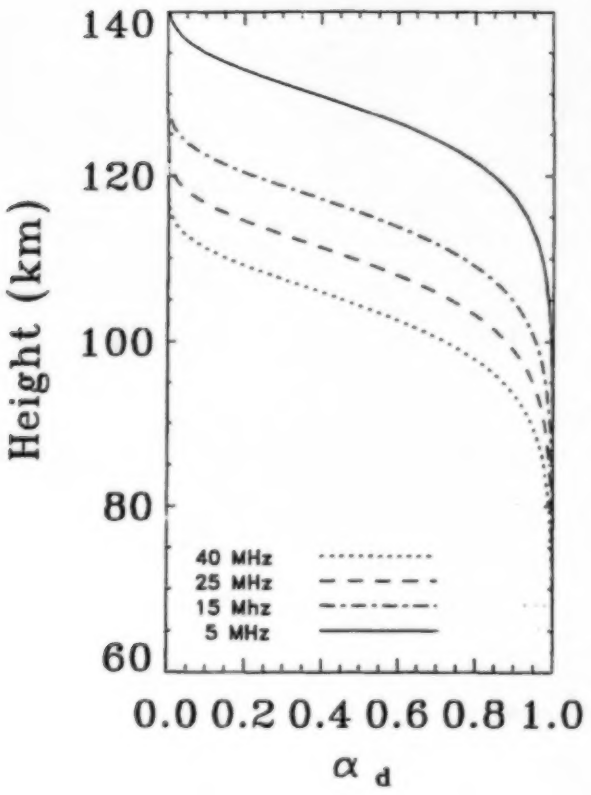


Figure 3: The height distribution of the amplitude attenuation factor, $\alpha_d$, due to diffusion for four different radar frequencies at PRF=100 Hz.

be seen by the radar. That is, rapid diffusion of the trail occurs between pulses so that the first observed echo is attenuated by this effect, making meteor detection less likely [*Steel and Elford,* 1991]. In addition, if the PRF is low the long duration of the echoes (because of the long decay time constant) leads to confusion between new meteor echoes, drifting meteor trails, multiple-bounce F-region/ground echoes, and patches of sporadic E-region ionization.

Therefore, the transmitter pulse repetition frequency must be sufficiently high so that the interval between pulses is always much less than the smallest decay time, $\tau_d$, likely to be observed for underdense echoes. Thus an attenuation factor incorporating the effect of diffusion during the inter-pulse period is necessary. This factor is given by:

$$\alpha_d = \exp\left(\frac{-16\,\pi^2\,D_a}{\lambda^2\,(\mathrm{PRF})}\right) = \exp\left(\frac{-1}{\tau_d(\mathrm{PRF})}\right) \tag{9}$$

where the PRF is in Hz [*Steel and Elford,* 1991]. This assumes that the trail is formed just after the instant of passage of a transmitted pulse. A more precise expression for a particular experiment would be dependent upon the exact meteor recognition criteria used (e.g., single pulse return above some threshold, two successive pulses, a running average, etc.).

Figure 3 shows the height distribution of the amplitude attenuation factor due to diffusion, $\alpha_d$, for four different radar frequencies. The PRF used in this computation is PRF=100 Hz. The figure clearly illustrates that $\alpha_d$ is very sensitive to the radar frequency and altitude. As an example, if $h = 91$ km, then $D_a = 2.44$ m$^2$s$^{-1}$ and so for $\lambda = 12$ m, we find $\alpha_d = 0.97$. At 115 km, $\alpha_d$ is dramatically reduced to about 0.17. This shows that detectable echo amplitudes at 12 m radar wavelength are very unlikely above 115 km. At 91 km, the decay time constant is 0.37 s. Underdense trails at observable heights therefore have duration of about a few tenths of a second. In contrast to 91 km, at a height of 115 km the time decay constant is reduced to about 6 ms and trails become very difficult to detect unless the radar wavelength is increased. For example, at $\lambda = 60$ m and $h = 115$ km, the time decay constant has increased to about 0.14 s.

### 2.1.2 Wind-induced effects

In addition to ambipolar diffusion rate, there are other processes such as wind induced effects, magnetic effects, and chemical effects, which might affect the measured diffusion rate. The geocentric velocity of meteoroids is very much greater than that of the winds in the meteor region so that the meteor trail is substantially straight at the moment of its formation. Although much of the standard theory of the reflection of radio waves from meteor trails has been based on a straight-trail model, it has been generally recognized that the reflection process can be altered as the result of wind-induced distortions of the trail, which becomes progressively more pronounced with time. It is found that the amplitude of the echo is influenced by (a) the wind shear, which shifts the reflection point along the non-uniformly ionized trail, (b) the wind shear gradient, which bends the trail and thus causes some degree of focussing, (c) small-scale wind shears, which cause the trail to become wrinkled so that the spatial coherence of the reflected wave is reduced, and (d) secondary reflection points, which appear when the large scale distortion of the trail has become sufficiently marked

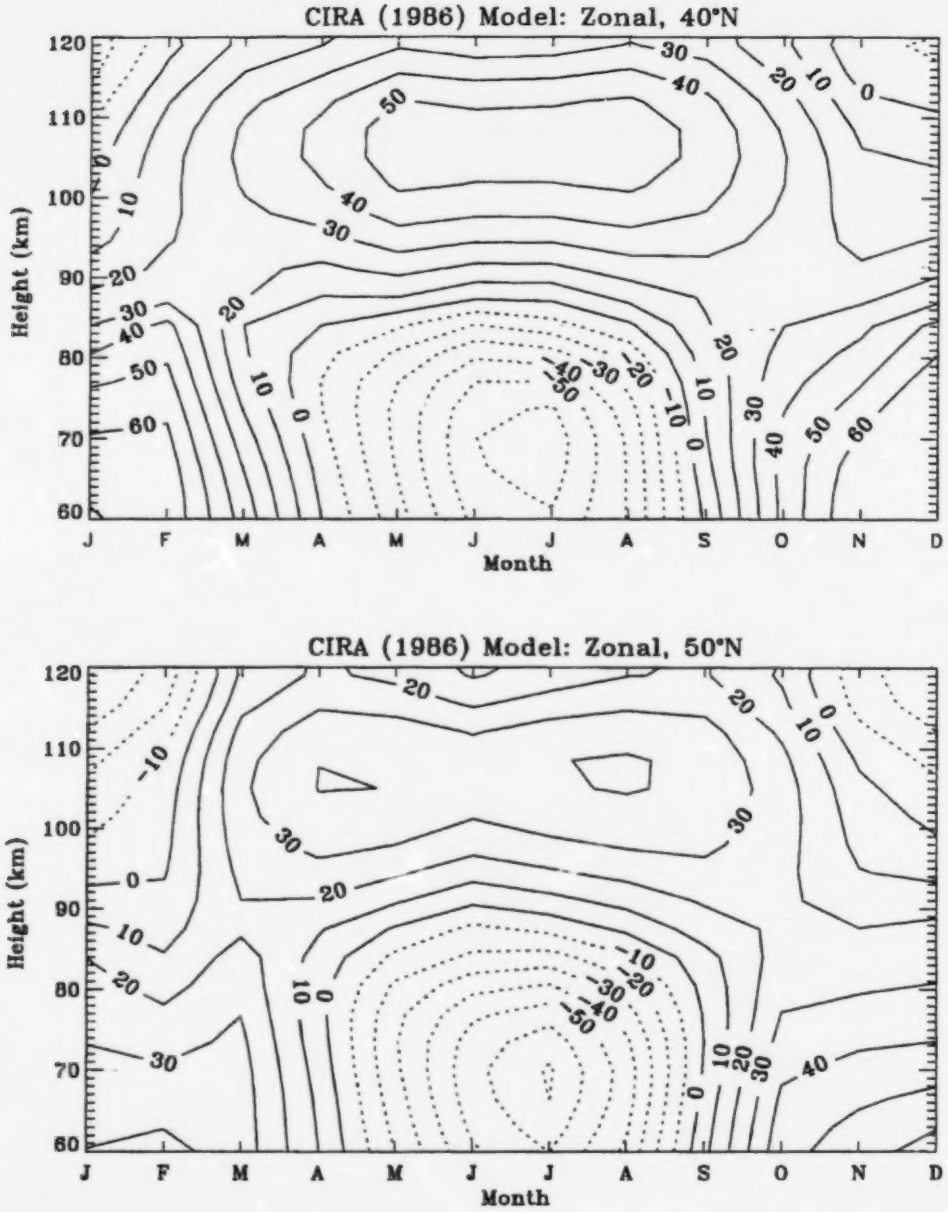


Figure 4: Contours of zonal mean winds in $ms^{-1}$ at latitudes for 40° N and 50° N.

[*McIntosh,* 1969; *Phillips,* 1969; *Jones,* 1975]. It is noteworthy that for wavelengths below 15 m (or frequencies above 20 MHz) the decay time is short compared to the time taken for the wind to distort the trail from its initial straight line. However, at long wavelengths (or low frequencies, e.g., 2 MHz) this is no longer the case and most trails are influenced by wind-induced effects during the life time of the echo.

Figure 4 presents the zonal monthly mean winds from the empirical model of *Fleming et al.* [1988] in the meteor height region at latitudes for 40° N and 50°N. Note that the comparison between these two latitudes is ideal because our latitude is 45° N. When a wind component is resolved into geographic coordinates, a positive wind amplitude refers to a wind directed towards the east or north for the zonal and meridional components, respectively. The meridional monthly mean wind is not presented since this component is very small and variable in this height range and thus no empirical model is available for this component in the literature. Figure 4 illustrates that in the spring and summer months, from April to August, the zonal flow is westward at heights below 90 km, reversing to an eastward flow above this height. The change-over from winter to summer circulation commences during April-May, and the summer to winter circulation commences during August-September. In the fall and winter, from September to February, the zonal flow is strongly eastward at most heights, being of greater amplitude below 80 km and decreasing with increasing height, but there is a tendency of reversal above 100 km during the winter time. The Figure 4, in general, shows that meteor trails are formed in an atmosphere that is in horizontal motion with speeds of the order of 10-60 $ms^{-1}$ and subject to wind shears that are typically 1-5 $ms^{-1}km^{-1}$.

Above 95 km, where the tranverse electron mobility is less than that of the ions, electrons tend to move preferentially along the magnetic field lines and it was thought that this might strongly reduce the diffusion of meteor trail traverse to the magnetic field. The theoretical work of *Kaiser et al.* [1973] and *Jones* [1991] has shown that this is unlikely below 130 km except for meteor trails that are closely aligned with magnetic field. This effect diminishes very rapidly as the angle between the trail axis and the field lines is increased to about 2°. Above 130 km, where the ion gyromagnetic frequency is greater than the ion collision frequency, the diffusion of the ions traverse to the field lines is reduced but this is not important for a short wavelength radar since few meteors are observed above 100 km.

There are a number of chemical reactions which can result in the decrease of electron density within the trail and hence the amplitude of the radar echo [*Jones,* 1975]. Another influence,

(although of little importance here), is that meteors forming at heights of $\leq$ 78 km have a decreased probability of detection due to the rapid loss of ionization which itself is due to the transfer of charge from atomic oxygen ions, with molecular ions being formed [*Jones*, 1975; *Baggaley*, 1978, 1979].

There are two other main effects of note, one due to the initial radius of the meteor trail, and the other due to the finite meteor velocity. The next consideration is the width of the meteor trail, and how this varies with altitude.

## 2.2 Initial Radius of the Trail

The second factor concerns the finite values of the radii of the meteor trails in the initial stage of their formation, the presence of which causes attenuation of radio echo amplitudes. If the initial radius $r_0$, defined as the half-amplitude half-width of an assumed initial Gaussian distribution of electron density, is small compared with $\lambda/2\pi$, where $\lambda$ is the radar wavelength, the scattering coefficient for underdense trails is simply that appropriate to the condition that all electrons in any cross-section scatter in phase. However, when $r_0$ is finite, the initial trail will reduce the returned echo amplitude by a factor:

$$\alpha_r = \exp\left(\frac{-4\,\pi^2\,r_0^2}{\lambda^2}\right) \tag{10}$$

[e.g., *Baggaley*, 1970]. This initial radius is thought to be due to the fact that the evaporating meteoric species initially have forward velocities close to the translational velocity of the meteor (which is in the 12-72 km/s range), this being about two orders of magnitude higher than the diffusive velocities of atmospheric species in the meteor region [*Greenhow and Hall*, 1960; *McKinley*, 1961]. The meteoric atoms therefore spread at this high velocity until slowed down by collisions [*Bronshten*, 1983]. The meteor trail is therefore formed with a certain radius and this arises near instantaneously. The initial radius of the meteor trail, $r_0$, in the 80-120 km height range is approximated by:

$$\log_{10} r_0 = 0.019h + \log_{10}\left(\frac{V}{40}\right) - 1.92 \tag{11}$$

where $h$ is the height in km, $V$ is the meteor velocity in km/s, and $r_0$ is then in m [*Baggaley*,

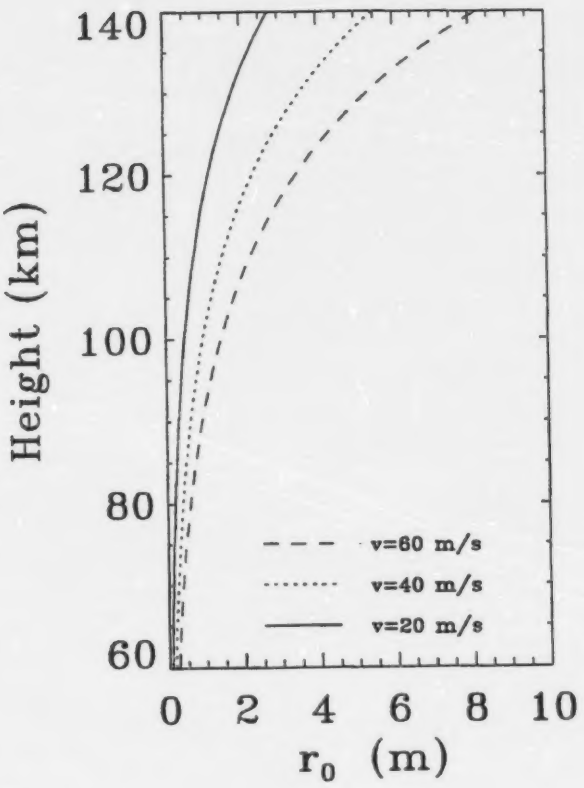


Figure 5: The height distribution of initial radius, $r_0$, for three different velocities.

1980, 1981].

Figure 5 shows the height distribution of initial radius for three different velocities. It is apparent that the initial radius grows rapidly with increasing altitude. The initial radius approximately doubles at all heights for an increase in velocity from 20 to 40 m/s and triples for an increase in velocity from 20 to 60 m/s at all heights. It is also interesting to note that the initial radius rises from about 0.5 m at 85 km altitude to 2 m at 115 km, for a velocity of 40 m/s.

Figure 6 shows the height distribution of the amplitude attenuation factor due to initial radius effect, $\alpha_r$, for three different velocities. Figure 6 also illustrates the comparison of $\alpha_r$

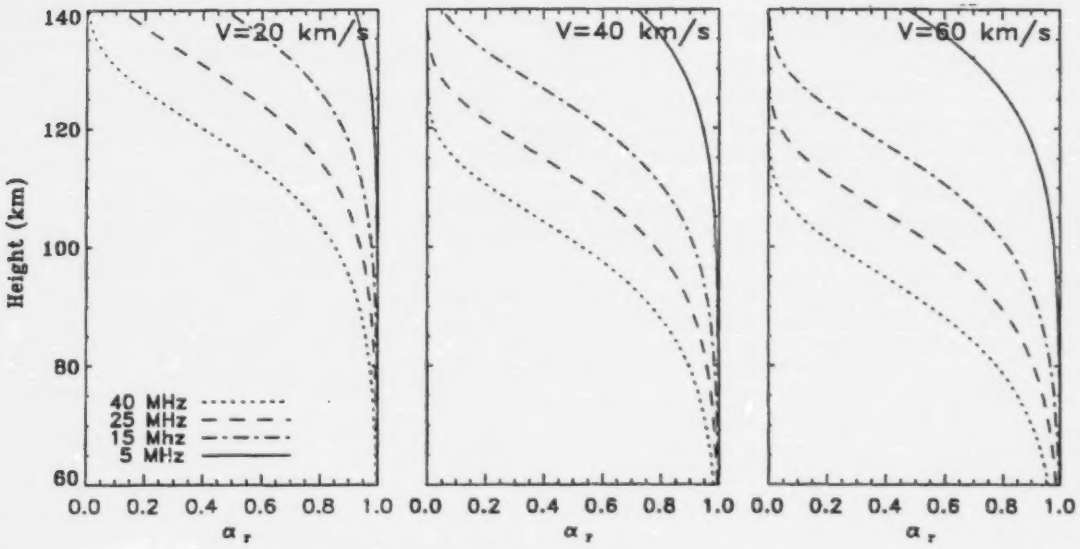


Figure 6: The height distribution of the amplitude attenuation factor, $\alpha_r$, due to initial radius effect for three different velocities.

at different radar frequencies of 5, 15, 25, and 40 MHz. The significance of radar frequency is clearly evident from the figure. As an example, if $V = 40$ km/s and $h = 95$ km (this height is taken as an example in this section because we shall see later that height distributions of the meteors peak around 95 km at 25 MHz radar frequency), then $r_0 = 0.77$ m and so for $\lambda = 12$ m the initial radius attenuation factor $\alpha_r$ is 0.85, while at $h = 120$ km, $\alpha_r = 0.24$. Considering only the initial radius effect, it can therefore be seen that a 12 m wavelength meteor radar has a very low probability of detecting any meteors forming above 120 km in height (Figure 6).

## 2.3 Finite Meteor Velocity

The third factor to be considered is the effect of the finite meteor velocity [*Kaiser*, 1953]. The radio echo is dominated by the contribution of the first Fresnel zone of the trail, which the meteor takes a finite time to cross. If, by the time the meteor has reached the end of this zone, the trail has diffused to reach a width comparable to the wavelength, then the echo amplitude will be severely attenuated. Clearly this effect depends upon the length of this

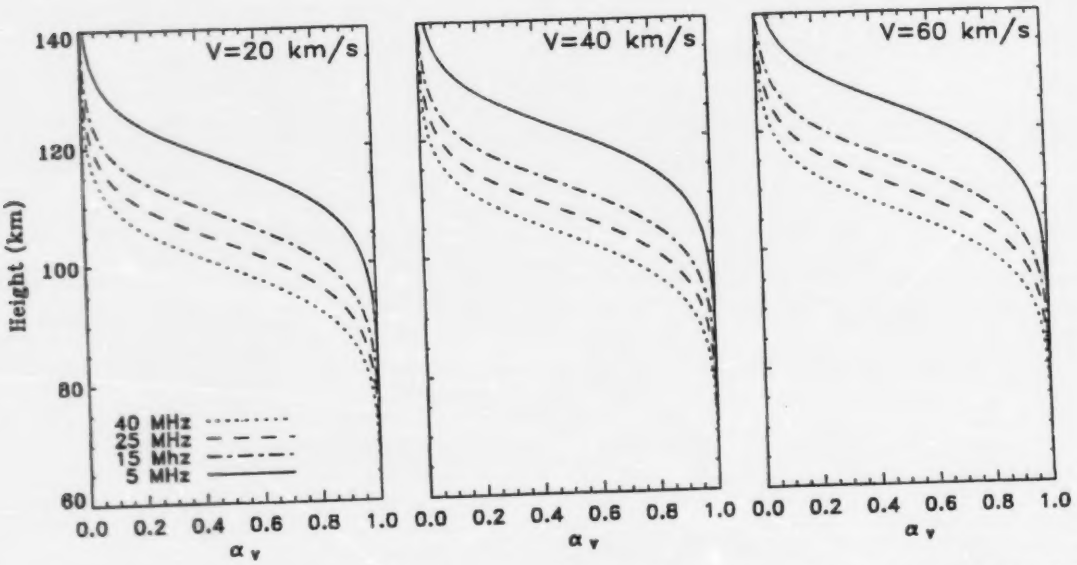


Figure 7: The height distribution of the amplitude attenuation factor, $\alpha_V$, due to finite velocity effect for three different velocities.

zone, 2 $(\frac{R\lambda}{2})^{\frac{1}{2}}$, where $R$ is the meteor range from the observatory site [e.g., *Greenhow and Hall*, 1960], the velocity, $V$, the diffusion coefficient, $D_a$, and the wavelength, $\lambda$. Note that $(\frac{R\lambda}{2})^{\frac{1}{2}}$ is the radius of the first Fresnel zone. The time, $t$, required for the meteor to traverse the first zonal zone is then $\frac{\sqrt{(R_0\lambda/2)}}{V}$. After substituting this value of $t$ in equation (3), the attenuation in echo amplitude is given by a factor

$$\alpha_V = \exp[-16\,\pi^2\,(\frac{D_a}{V})\,(\frac{R}{2\,\lambda^3})^{\frac{1}{2}}] \tag{12}$$

Thus, although the first Fresnel zone increases in length with wavelength, in fact the finite velocity effect is reduced by using a longer wavelength. The contribution from the $D_a/V$ term would naturally be greater if we use a smaller value of $V$, but in evaluating an over-all ceiling, a large $V$ value is more appropriate because high-velocity meteors ionize at greater heights than low-velocity meteors. It should be noted that the finite velocity effect has the opposite trend to the initial radius effect; at any particular height the former is more severe for slower meteors. Note also that $\alpha_V$ approaches unity as $V$ becomes very large.

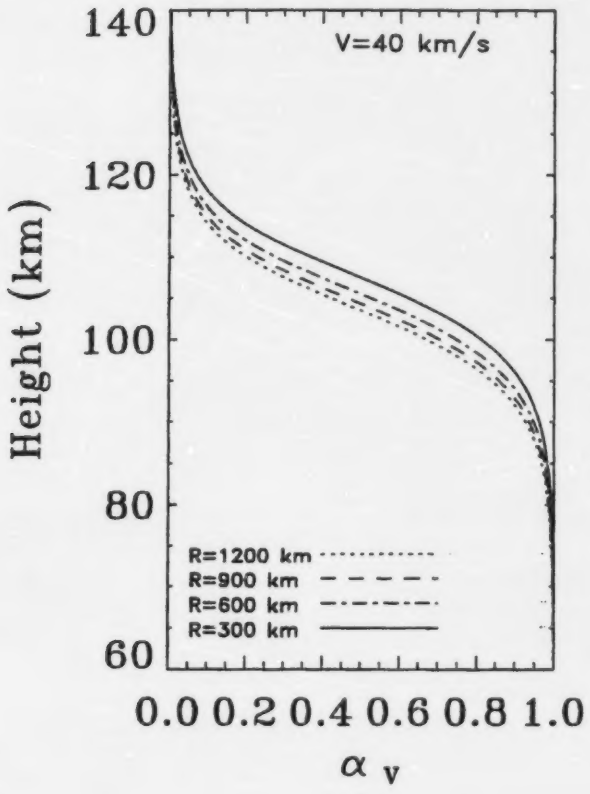


Figure 8: The height distribution of $\alpha_V$ as a function of range, $R$, for a radar frequency of 25 MHz and velocity of 40 m/s.

Figure 7 shows the height distribution of the amplitude attenuation factor due to finite velocity effect, $\alpha_V$, for three different velocities. Figure 7 also illustrates the comparison of $\alpha_V$ at different radar frequencies of 5, 15, 25, and 40 MHz. The importance of radar frequency is evident from the figure. The range used in the computation is R=300 km. As an example, if $V = 40$ km/s, and $h = 95$ km, $\alpha_V$ is 0.91, while at $h = 115$ km, $\alpha_V = 0.17$. Considering only the finite velocity effect, it can therefore be seen that a 12 m wavelength meteor radar has a very low probability of detecting any meteors forming above about 115 km (Figure 7).

Figure 8 shows the height distribution of $\alpha_V$ as a function of range, $R$, for a radar frequency

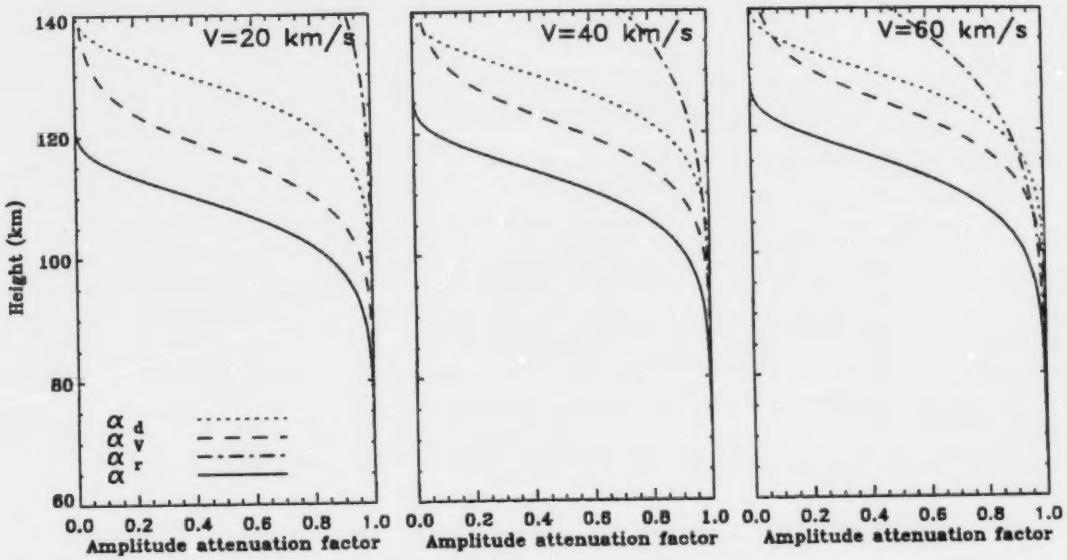


Figure 9: Amplitude attenuation factors at $f = 5$ MHz radar frequency. The values of the four $\alpha's$ are plotted as functions of height at three velocities (20, 40, 60 km/s). The pulse repetition frequency used is 100 Hz. The range used in the computation is $R = 300$ km.

of 25 MHz and velocity of 40 m/s. Clearly, the radar is insensitive to different range of underdense meteors.

## 2.4 Total Attenuation

The individual attenuation from equations (9), (10), and (12) give a total attenuation in the returned amplitude from an underdense meteor trail. Therefore, the total attenuation is given by:

$$\alpha = \alpha_r \, \alpha_V \, \alpha_d \tag{13}$$

Figure 9 shows the attenuations factors for a 5 MHz radar frequency. The values of the four $\alpha's$ are plotted as functions of height at three velocities (20, 40, 60 km/s). The pulse repetition frequency used is 100 Hz. The range used in the computation is $R = 300$ km. The total amplitude attenuation is 0.5 at $h \approx 110$ km for $V = 20$ km/s, and this height increases

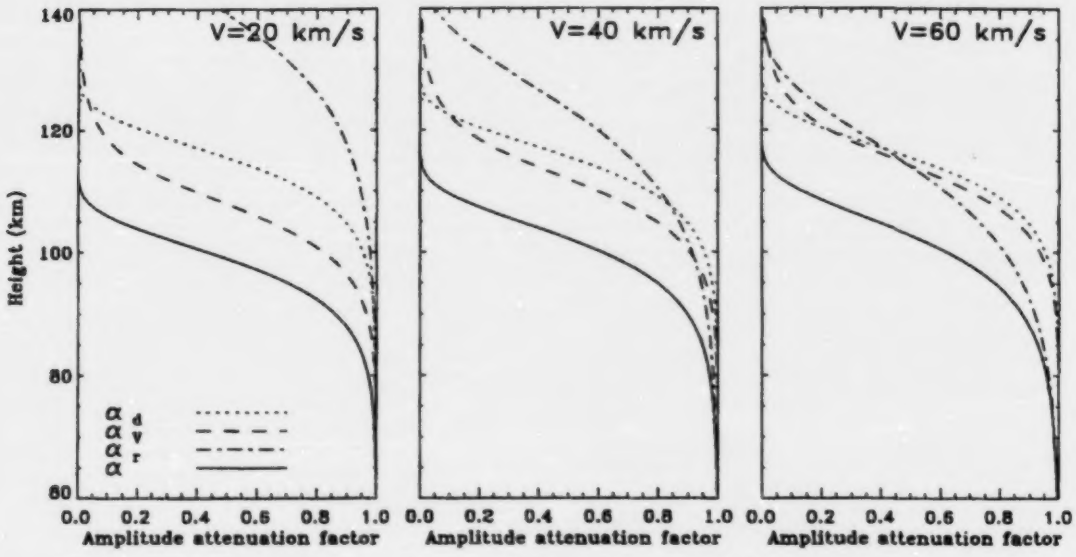


Figure 10: As for Figure 6 except $f = 15$ MHz.

to 112 and 114 km with increasing velocity. At $V = 20$ km/s, the finite velocity effect $\alpha_V$ dominates the net attenuation, whilst at the larger velocities the finite velocity effect term $\alpha_V$ and diffusion term $\alpha_d$ are more important. The initial radius effect is of no significance.

The plots are repeated for a 15 MHz radar frequency in Figure 10, again with the same PRF and range. Since the finite velocity effect term is the most significant throughout, the diffusion term and initial radius effect are more important with increasing velocity. At $V = 60$ km/s, all three terms are equally important. At lower heights, the total amplitude attenuation is controlled by the initial radius effect with increasing velocity. The height at which $\alpha = 0.5$ increases from 99 to 101 to 103 km with increasing velocity.

Figure 11 shows the attenuation factors for a 25 MHz radar frequency. At low velocity $\alpha_V$ is dominant, however, at $V = 40$ km/s all three terms are equally important. But at $V = 60$ km/s the initial radius term $\alpha_r$ dominates. The height at which $\alpha = 0.5$ increases from 94 to 96 to 98 km with increasing velocity.

Figure 12 shows the attenuation factors for a 40 MHz radar. At $V = 20$ km/s, $\alpha_V$ dominates the net attenuation but at $V = 40$ km/s, the initial radius term $\alpha_r$ has taken control and at

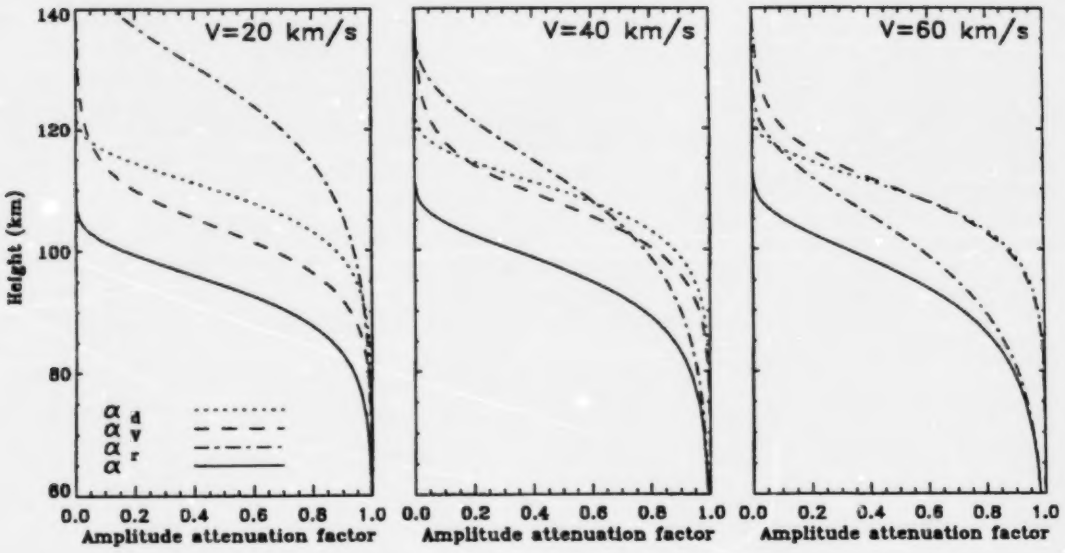


Figure 11: As for Figure 6 except $f = 25$ MHz.

$V = 60$ km/s the initial radius term totally dominates the amplitude attenuation factor.

## 2.5 Sampling Time Interval

The data processing scheme is important to detect underdense meteors at particular radar frequency. As an example, a 40 km/s meteor at range 300 km takes $\sim 0.067$ s ($\approx \frac{2\sqrt{R\lambda/2}}{V}$) to cross the first Fresnel zone at 12 m radar wavelength, so that the rise of the echo is comparatively rapid. All rise times would be less than 0.224 s, corresponding to a meteor velocity of 12 km/s. The decay time constants for $\lambda = 12$ m are $\sim 2.546$ s at 80 km, $\sim 0.22$ s at 94 km, and $\sim 0.008$ s at 113 km (see Figure 2). Therefore, the meteor echo must persist for $> 2.77$ s to be recognized above 80 km, and so data interval of 3 s is considered to be a good choice. The sampling time interval (time duration between successive points) is 0.01 s when using 100 Hz PRF (here we assume that PRF is equal to the sampling interval). This indicates that some echoes above 113 km will be rejected by the processing. That is, the returned echo amplitude is sufficient for detection but the data processing scheme causes some of these high altitude meteors to not be recorded.

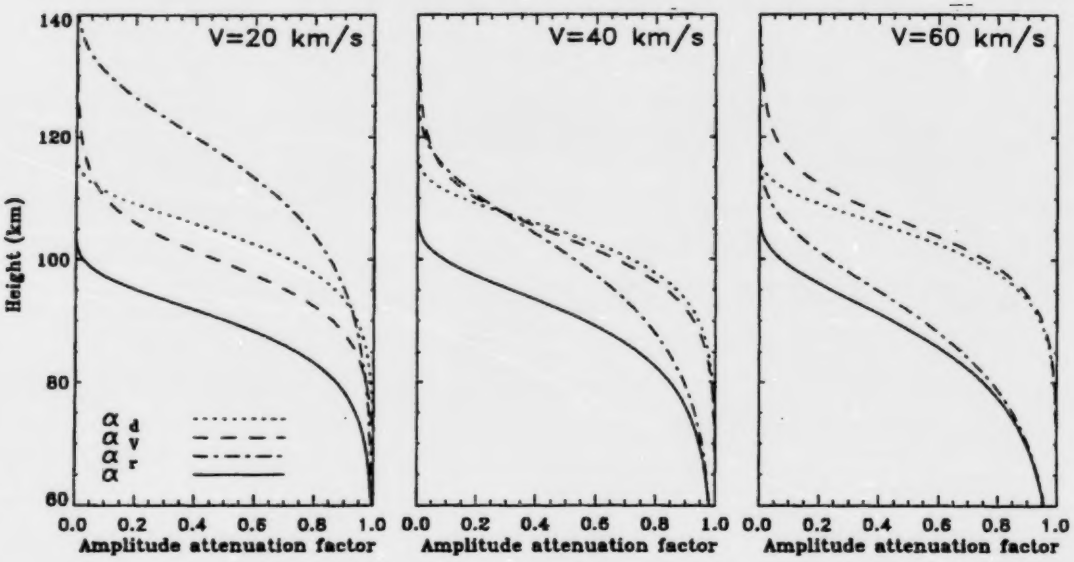


Figure 12: As for Figure 6 except $f = 40$ MHz.

# 3 Radio wave backscattering from an underdense meteor trail

Radar can readily detect the electrons in meteor trails. In the case of a backscatter radar, where the transmitter and receiver are at the same location, an echo is observed only if the meteor trail is at right angles to the radar beam. The radar echo technique measures the electron line density in the vicinity of the specular reflection point. Consider a trail of uniform ionization whose diameter is small compared to the wavelength and where the effect of diffusion during the formation period of the trail can be ignored. Figure 13 illustrates the reflection geometry. Once created the trail, extends from $s = -\infty$ to $s = +\infty$, where $s$ is distance measured along the meteor path relative to an origin at the minimum range point $(R_0, t_0)$. Thus, we have:

$$R^2 = R_0^2 + s^2 = R_0^2 + V^2 (t - t_0) \tag{14}$$

The incident radio wave penetrates the column and is scattered by the individual free elec-

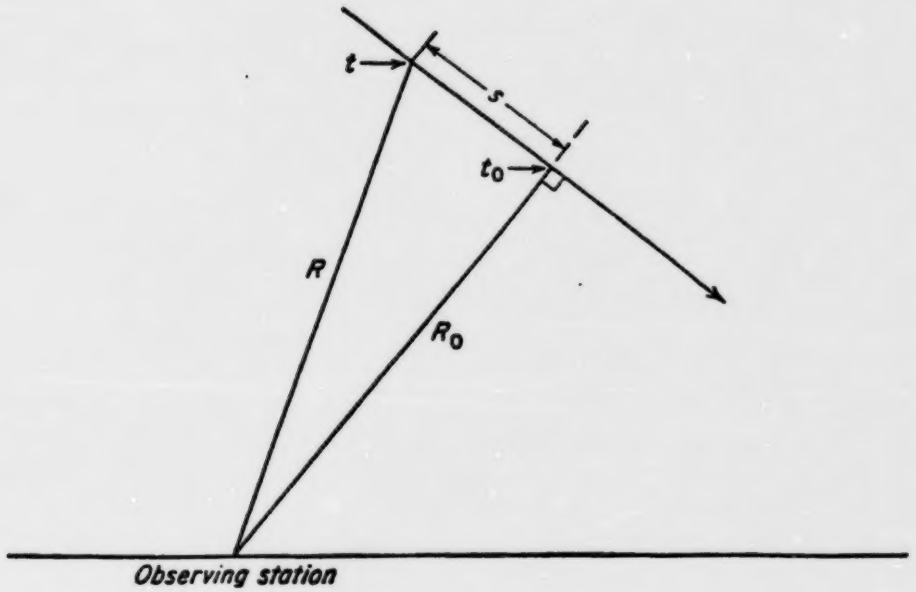


Figure 13: The geometry of the meteor path relative to the observing station.

trons, which oscillate freely in the applied field without colliding with other particles to any great extent. Each electron behaves as if no other were present, secondary radiative and absorptive effects may be neglected. This condition defines the underdense trail. The equivalent echoing area, or scattering cross-section of a free electron is:

$$\sigma_e = 4\pi r_e^2 \sin^2\gamma \tag{15}$$

[e.g., *Brekke,* 1977] where $r_e$ is the classical electron radius and $\gamma$ is the angle between the electric vector of the incident wave and the line of sight of the receiver. For the case of

backscatter $\gamma = \pi/2$ and $\sigma_e \approx 1.0 \times 10^{-28}$ m$^2$.

At a point on a trail distance $R$ from a radio transmitter, the power flux of the incident wave is:

$$\Phi_i = \frac{P_T G}{4\pi R^2} \quad \mathrm{Wm}^{-2} \tag{16}$$

[*Skolnik*, 1990] where $P_T$ is the transmitted power and $G$ is the antenna gain relative to an isotropic radiator, in the direction of the trail element. Assuming that the same or an identical antenna is used for reception, the effective absorbing area of the antenna is $G\lambda^2/4\pi$ when the antenna impedance is matched to the receiver. Thus the power delivered at the receiving antenna of radiation scattered from the single electron is [*Skolnik*, 1990]:

$$\Delta P_R = \frac{P_T G}{4\pi R^2} \frac{\sigma_e}{4\pi R^2} \frac{G\lambda^2}{4\pi} = \frac{P_T G^2 \lambda^2 \sigma_e}{64\pi^3 R^4} \tag{17}$$

In a trail whose diameter is small compared to the wavelength, all electrons can be assumed to be on the axis, and thus all those in a line element $ds$ scatter in phase. We must add their electric field vectors rather than their power fluxes. In order to sum the resultant returned radiation at the receiving antenna an electric field $\Delta\vec{E}_R$ is associated with each scalar quantity $\Delta P_R$, such that the maximum amplitude of the electric field $\Delta E_0$, is given by $\Delta E_0 = (2Z_0\Delta P_R)^{1/2}$ where $Z_0$ is the wave impedance of free space (i.e., 377$\Omega$) [*Sander and Reed*, 1986; *Edminister*, 1993]. Moreover, each electric field vector has a phase delay of $2kR$ radians, relative to the transmitted radiation, where $k = 2\pi/\lambda$. If the trail has a line density of $q$ electrons per meter, the instantaneous amplitude of the field due to the $q\ ds$ electrons in the trail element $ds$ is given by $(2Z_0\Delta P_R)^{1/2} \exp j(\omega t - 2kR) q\ ds$ [*Hoole*, 1990]. As $R$ changes with time, a phase modulation of the wave is produced. Hence the amplitude $E_R$, of the field at the receiving antenna due to scattering from the whole trail is given by:

$$E_R = (2Z_0\Delta P_R)^{1/2} q \int \exp j(\omega t - 2kR)\ ds \tag{18}$$

where the integral is taken over the length of the trail. The parameter $q$ may be taken out from the integral sign only if we assume it to be constant along the trail.

In general the change in range is small compared to the orthogonal distance $R_0$ to the

trail, so that the approximation $R \cong R_0 + s^2/(2R_0)$ can apply, where $s$ is the distance along the trail from the orthogonal point ('$t_0$ point') to $ds$ [Figure 13]. For convenience, we employ the substitution $\pi x^2/2 = ks^2/R_0$, the phase factor becomes $\omega t - \pi x^2/2 - 2kR_0$, and $ds = (R_0\lambda/4)^{1/2}\, dx$, Thus the expression for $E_R$ becomes

$$E_R = (\frac{R_0\lambda}{4})^{1/2}\,(2Z_0\Delta P_R)^{1/2}\,q\,\exp j(\omega t - 2kR_0)\int \exp j(\frac{-\pi x^2}{2})\,dx \tag{19}$$

or

$$E_R = (\frac{R_0\lambda}{4})^{1/2}\,(2Z_0\Delta P_R)^{1/2}\,q\,\exp j(\omega t - 2kR_0)\,(C - jS) \tag{20}$$

where $C$ and $S$ are the conventional Fresnel integrals of optical diffraction theory [e.g., *McKinley,* 1961],

$$C = \int \cos(\frac{\pi x^2}{2})\,dx \quad \text{and} \quad S = \int \sin(\frac{\pi x^2}{2})\,dx. \tag{21}$$

Therefore the power delivered to the receiver by scattering from the whole trail is:

$$P_R = \frac{E_R^2}{2\,Z_0} = \frac{\Delta P_R\, R_0\,\lambda}{2}\,(\frac{C^2 + S^2}{2})\,q^2 \tag{22}$$

Whence, on substituting for $\Delta P_R$ from equation (17), the received power is

$$P_R = \frac{P_T\,G^2\,\lambda^3\,\sigma_e}{128\,\pi^3\,R_0^3}\,(\frac{C^2 + S^2}{2})\,q^2 \tag{23}$$

or

$$P_R = 2.5 \times 10^{-32}\,P_T\,G^2\,(\frac{\lambda}{R_0})^3\,(\frac{C^2 + S^2}{2})q^2 \tag{24}$$

This is the basic expression for the echo power received from the underdense trail once the whole trail is formed. Note that the orthogonal range $R_0$ can be used in place of all $R$, with negligible error. The value of $C^2 + S^2$ is 2 when evaluated from $s = -\infty$ to $+\infty$. The

approximation that we used for $R$ does not permit us to go very far in either direction from $t_0$ point, but it can be shown that the contribution from the remoter parts of the trail are negligible and that the value of $C^2 + S^2$ is close to 2 when taken over a few Fresnel zones on both sides of $t_0$. Therefore, the received power is given in watts by

$$P_R = 2.5 \times 10^{-32} \, P_T G^2 \, (\frac{\lambda}{R_0})^3 \, q^2 \tag{25}$$

It should be noted that the above equation has a range dependence of $R^{-3}$ which lies between the cases of a hard target ($R^{-4}$) and distributed targets ($R^{-2}$) [*Sato,* 1989]. In the above relation, since it is assumed that trails are of infinite length, every trail has a first Fresnel zone and therefore gives a reflection. In practice, however, since trails are of finite length, this zone may not lie on the trail but rather on an extension of it. In such a case the signal returned from the trail will be a relatively weak one, and in practice these returns are of little importance. Thus a radar can 'see' only a fraction of all the trails incident on the atmosphere within its range because most trails do not have the proper orientation for the radar line-of-sight to be perpendicular to the trail. The requirement for proper orientation can be restated as requiring that the trail be tangent to a sphere centered at the radar.

The wavelength used for the radar detection of meteors must be considerably larger than the trail width, otherwise interference between reflections from the front and back of the trail would result in a very low returned power. Thus the maximum frequency that can used is around 100 MHz [*Hughes,* 1978]. It can be seen from equation (25) that the reflected power is proportional to $\lambda^3$, so high-frequency work requires high-powered transmitters and sensitive receivers. Only man-made interference and the ever increasing size of aerials limit the lower end of the frequency range used. Most meteor work is done with frequencies between 20 MHz and 60 MHz.

# 4 Height Distribution of Meteors

The initial echo power in watts, from underdense reflection, assuming that the initial trail radius to be much smaller than the wavelength employed, is given by the radar equation (25). In this report, we confine ourselves to echoes backscattered from underdense trails, undistorted by effects such as windshears. The attenuation factors discussed in Section 2

mean that the expression (25) for the initial echo power must be modified to become:

$$P_R = 2.5 \times 10^{-32}\, P_T G^2\, (\frac{\lambda}{R})^3\, \alpha^2\, q^2 \tag{26}$$

The received amplitude is thus

$$A = (\text{const.})\alpha q \tag{27}$$

The number of meteors detected will depend upon how many give rise to an amplitude above some threshold value, $A_{\min}$. Thus at some height $h$

$$N(\text{detected at } h) = N(h, \{A > A_{\min}\}) = N(h, \{\alpha q > (\alpha q)_{\min}\}) \tag{28}$$

and since for a certain velocity the height defines $\alpha$,

$$N(\text{detected at } h) = \alpha N(h, \{q > q_{\min}\}) \tag{29}$$

so that for a particular limiting line density $q_{\min}$,

$$N(\text{detected at } h) = \alpha N(h) \tag{30}$$

where $N(h)$ is the true height distribution which is not directly determined.

For the present purpose the simple model of *Steel and Elford* [1991] will be used in this report. This model, normalized to the peak, is:

$$N(72 < h < 105\,\text{km}) = [(h - 72)/44]^2 \tag{31}$$

and

$$N(105 < h < 140\,\text{km}) = 1 \tag{32}$$

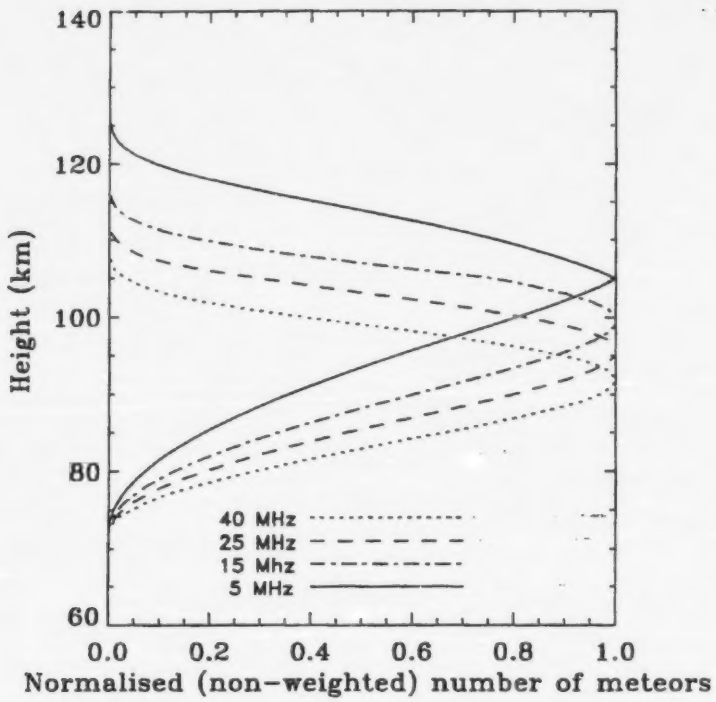


Figure 14: Height distributions of underdense meteor trails at radar frequencies of 5, 15, 25, and 40 MHz.

This model is based on previous observations at different frequencies in the 2-55 MHz range [*Steel and Elford,* 1991]. This model incorporates an assumed meteor flux variation with height and attenuation of the returned echo amplitude due to the initial trail radius, the finite meteor velocity, and also the radial diffusion. Figure 14 shows the height distributions of underdense meteor trails at frequencies of 5, 15, 25, and 40 MHz. The velocity used in this computation is $V = 40$ km/s. The height distributions at 25 and 40 MHz are typical of VHF meteor radars, with the maximum number of meteor echoes occurring near 95 and 92 km, respectively, and the number of echoes falling off rapidly above this peak height. It is noteworthy that above this peak height the diffusion reduces the echo duration, while below it attachment and wind turbulence become increasingly important. The model height of maximum echo rate is consistent with other meteor radar observations, with peaks below 100 km and few meteors detected above 105 km [e.g., *Hess and Geller,* 1977; *Tetenbaum et al.,* 1986; *Wang et al.,* 1988; *Steel and Elford,* 1991; *Reddi et al.,* 1993]. The height of

maximum echo rate predicted by the model at 5 and 15 MHz are 105 and 100 km, respectively. The main features of the measured height distributions are also predicted, with peak at 105 km for a 5 MHz radar [e.g., *Elford and Steel,* 1988]. The model indicates few 5 MHz echoes above 115 km.

The resultant effect of a trail's initial radius, finite velocity of formation and diffusion is a significant attenuation of the radar echo so that an effective 'ceiling' of about 110 km occurs for observations at 25 MHz (corresponds to 12 m wavelength), rising to 120-130 km at 5 MHz. Thus, the average echo height of meteors becomes a function of frequency and can be described by:

$$h = -17 \log_{10} f + 119 \tag{33}$$

where $h$ is in km and $f$ is in MHz. As an example, at 25 MHz, $h$ is 95 km and at 40 MHz, $h$ is 92 km.

# 5 Radar Detection of Meteors at Low Frequency

Most meteor radars have customarily been operated at radio frequencies of around 20-60 MHz (5-15 m wavelengths) in order to avoid problems associated with reflection or absorption of the radio wave in the ionosphere. It is suggested that the 'missing mass' in the $10^{-6} - 10^{-2}$ g range of interplanetary material might be held in a faint, high velocity component which could be undetected since it ablates at high altitudes [*Hughes,* 1978]. *Hughes* [1978] argued that only $3-4\%$ of the meteoric mass incident upon the upper atmosphere in the $10^{-6} - 10^{-2}$ g range is being detected by conventional radio meteor techniques. This would imply that the vast majority of meteoric material is deposited into the atmosphere above 100 km, having important ramifications for aeronomy and other branches of the atmospheric sciences. The existence of such high velocity, low mass meteors would also be significant in relation to the origin and evolution of the meteoroidal complex in the solar system.

Conventional meteor radars, operating at wavelengths of around 5-15 m (20-60 MHz frequency), are unable to detect high altitude meteors due to the wavelength dependent echo ceiling (see Section 4). The diameter (or width) $r_0$ of an underdense ionized trail increases monotonically with height in the 80-140 km region due to the increase in the molecular mean

free path with diminishing air density. Consequently, a rapid growth with height occurs both in the initial radius of a forming trail and also in its rate of expansion due to the mechanism of ambipolar diffusion $D_a$ during the finite time required for the meteor to traverse the central (first) Fresnel zone of the radar (so-called finite velocity effect, also see Section 2.3). The echo ceiling begins to act at heights for which the diameter of a trail approaches the dimensions of an appreciable fraction of the wavelength, when destructive interference between waves reflected from the front and back of the trail's cylindrical cross-section causes increasing attenuation of the backscattered signal.

However, recently there have been many observations of the meteors at frequencies below 20 MHz [e.g., *Olsson-Steel and Elford,* 1987; *Elford and Olsson-Steel,* 1988; *Thomas et al.,* 1988]. Radars employing such frequencies are potentially able to detect many more underdense meteor echoes than the radars operating at the more conventional higher frequencies. This occurs as a consequence of the greater limiting height for the detection of echoes at longer wavelengths which is set by the so-called underdense ceiling [*Greenhow and Hall,* 1960; *Olsson-Steel and Elford,* 1987; *Thomas et al.,* 1988]. *Olsson-Steel and Elford* [1987] studied the heights of radio meteors at a wavelength of 150 m (2 MHz frequency), for which the echo ceiling is above 140 km. Most observations were made between 0300 and 0700 hours local time due to ionospheric activity, which gives rise to other echoes which could be confused with meteors. They found that the height distribution of radio meteors peaks at $\sim$ 104 km. This is approximately 10 km higher than found from measurements at conventional wavelengths, due to the fact that these have a low probability of detecting high altitude meteors. They also found a substantial numbers of meteors above this peak (104 km), right up to the 140 km instrumental limit. Further, there is no sudden drop-off in numbers of meteors above the peak at 104 km. Therefore, they concluded that the 'missing mass', comprising the vast majority of the meteoric input to the atmosphere, ablates well above 100 km. It is noteworthy that the above results have a weakness of large uncertainty in the height determination; the uncertainty in individual meteor heights is $\pm$7 km, due to the inaccuracy of phase measurements. These observations were further substantiated by *Elford and Olsson-Steel* [1988]. They have measured the height distribution of radio meteors at a frequency of 6 MHz which has the instrumental limitations of heights to $84 < h < 116$ km. In this case, the measurements were only made between 0800 and 1600 hours local time, due to broadcast interference from a distant transmitter operating at almost exactly the same frequency as the radar. They found the peak at $\sim$ 105 km, and in line with observations made at 2 MHz [*Olsson-Steel and Elford,* 1987]. Unlike at 2 MHz, the 6 MHz height distribution of

meteors appears to be symmetric about the peak with a quite rapid drop-off in the number of meteors detected above 105 km. The origin of this difference is probably due to the finite velocity of the meteors and diffusion effects [*Elford and Olsson-Steel,* 1988].

There are many factors influencing the observation of meteors at low radio frequencies (2-6 MHz). Whilst the neutral atmosphere has little effect upon the propagation of radio waves in the VHF band, in the MF-HF band it can cause significant retardation, refraction, absorption and reflection of the waves. Therefore, an experiment with the low frequency radar is not an easy task. The influences of the retardation and refraction could lead to the virtual height of the meteor trail being considerably higher than its true height [e.g., *Namboothiri et al.,* 1993]. The retardation arises whenever the background electron density approaches the critical density. Thus the transmitted pulse cannot be assumed to propagate with constant speed at the velocity of light in a vacuum. So the virtual height for a given frequency is always greater than the true height. The refraction can also lead to the actual reflection point being displaced from that expected from linear geometry; that is the zenith angle of the ray path at the reflection point could differ from the zenith angle of the ray path at the ground.

Absorption can lead to attenuation of the returned echo signal in this frequency range (2-6 MHz), and hence leaving some meteors undetected. Severe ionospheric absorption sometimes occurs during the day, and also to a certain extent at night due to a substantial degree of ionization present above 80 km. During the daytime the large background electron density in the D- and E-regions make any observations unlikely. Sporadic E ionization could exist throughout some nights, making observations equally improbable. However, at night during the winter and spring months the ionization often falls to a level sufficiently low for meteor echoes to be detected [*Brown,* 1976]. Observations at a low radio frequency can be made at night if the amount of ionization below the E-region falls to a sufficiently low level, and using a right-hand circularly polarized transmitted beam for which absorption is very small [*Steel and Elford,* 1991]. For such observations the observational 'ceiling' would be raised so that the observed height distribution of the echoes should be much closer to the true height distribution of the trails.

Strong ionospheric reflections from the meteor region generally occur until about 0200 hours local time, and the morning development of the E-layer occurs quite rapidly after sunrise [*Olsson-Steel and Elford,* 1987]. Generally, no observations are possible after about 0800 hours local time, and often an earlier cut-off is necessary. Even during the night time the

background noise (for meteor-detection purposes) is not normally due to the receiver or antenna noise, but rather to weak ionospheric reflections which fluctuate rapidly [*Olsson-Steel and Elford,* 1987]. The presence of F-region echoes, with multiple bounces lasting for 3-4 ms, can lead to confusion with meteor echoes. In this case, a low pulse repetition frequency (e.g., 20-25 Hz frequency or 0.04-0.05 s interval between pulses) is desirable in order to obviate confusion due to multiple bounce F-region/ground echoes. On the other hand, the low PRF pulses are unable to detect the fast decaying echoes so that the number of meteor echoes will be greatly reduced and at higher altitudes the reduction is even more severe (see Section 2.1.1).

# 6 Conclusion

The strengths and limitations of radar detection of meteors at different radar frequencies have been studied based on standard theory. The standard theory takes into account of the initial trail radius, the finite meteor velocity, and the radial diffusion. The significance of the data processing scheme, the pulse repetition frequency, and the data sampling interval have all been highlighted in order to detect underdense meteor echoes.

We have developed a numerical model which is able to predict the height distribution of underdense meteors as a function of radar frequency. The study shows that radars operating at wavelengths of around 5-15 m are unable to detect high altitude meteors due to wavelength dependent ceiling. Long wavelength radars operating around 15-60 m are potentially able to detect many more underdense meteor echoes than the radars operating around 5-15 m. However, there are many important and attributive factors influencing the observation of meteors at low radio frequencies and the advantages and drawbacks are specifically discussed in so far as detecting meteors at low frequency.

# References


[1] Anderson, S. J., Remote sensing with the JINDALEE skywave radar, *IEEE J. Ocean. Eng.*, Vol. OE-11, no. 2, Apr., 158-163, 1986.

[2] Appleton, E. V., and M. A. F. Barnett, On some direct evidence for downward atmospheric reflection of electric rays, *Proc. Roy. Sco.*, A 109, 621-641, 1925.

[3] Avery, S. K., A. C. Riddle, and B. B. Balsley, The Poker Flat, Alaska, MST radar as a meteor radar, *Radio, Sci.*, 18, 1021-1027, 1983.

[4] Baggaley, W. J., On the variation of the ambipolar diffusion coefficient with height, *Planet. Space Sci.*, 18, 1836-1842, 1970.

[5] Baggaley, W. J., *Planet. Space Sci.*, 26, 1978.

[6] Baggaley, W. J., LF radiowave propagation effects of meteoric ionization, *Planet. Space Sci.*, 27, 533-535, 1979.

[7] Baggaley, W. J., Measurements of the velocity dependence of the initial radii of meteor trains, *Bull. Astron. Inst. Czechosl.*, 31, 308-311, 1980.

[8] Baggaley, W. J., Single wavelength measurements of the initial radii of radio meteor ionization columns, *Bull. Astron. Inst. Czechosl.*, 32, 345-349, 1981.

[9] Bittencourt, J. A., Fundamentals of plasma physics, *Pergamon press*, Toronto, Canada, 1986.

[10] Booker, H. G., Turbulence in the ionosphere with applications to meteor trails, radio star, scintillations, auroral radar echoes, and other phenomena, *J. Geophys. Res.*, 61, 673-705, 1956.

[11] Bronsthen, V. A., Physics of meteoric phenomena, *Reidel*, Dordrecht, 1983.

[12] Brown, N., Radio echoes from meteor trains at a frequency of 1.98 MHz, *J. Atmos. Terr. Phys.*, 38, 83-87, 1976.

[13] Brekke, A., Radar probing of the auroral plasma, *Scandinavian university books*, Universitetsforlaget Oslo, Norway, 1977.

[14] Chan, H. C., Detection and tracking of low-altitude aircraft using HF surface-wave radar, Defence Research Establishment Ottawa, Report No. 1334, December, 1998.

[15] Caswell, R. D., N. McBride, and A. D. Taylor, Olympus end of life anomaly - a Perseid meteoroid impact event ?, *Int. J. Impact Engng.*, 17, 139-150, 1995.

[16] Chilson, P. B., P. Czechowsky, and G. Schmidt, A comparison of ambipolar diffusion coefficients in meteor trains using VHF radar and UV lidar, *Geophys.Res. Lett.*, 23, 2745-1748, 1996.

[17] Davies, J. G., and C. D. Ellyett, The diffraction of radio waves from meteor trials and the measurement of meteor velocities, *Phil. Mag.*, (7) 40, 614-626, 1949.

[18] Edminister, J. A., Theory and problems of electromagnetics, *McGraw-Hill publishing company*, Toronto, Canada, 1993.

[19] Elford, W. G., and D. Olsson-Steel, The height distribution of radio meteors: observations at 6 MHz, *J. Atmos. Terr. Phys.*, 50, 811-818, 1988.

[20] Greenhow, J. S., Characteristics of radio echoes from meteor trails: the behaviour of the electron trails after formation, *Proc. Phys. Sco.*, 65, 169-181, 1952.

[21] Greenhow, J. S., and E. L. Neufeld, The diffusion of ionized meteor trails in the upper atmosphere, *J. Atmos. Terr. Phys.*, 6, 133-140, 1955.

[22] Greenhow, J. S., and J. E. Hall, *J. Atmos. Terr. Phys.*, 5, 109, 1955.

[23] Greenhow, J. S., and J. E. Hall, The importance of initial trail radius on the apparent height and number distributions of meteor echoes, *Mon. Not. R. Astr. Soc.*, 121, 183-196, 1960.

[24] Grossi, M. D., R. B. Southworth, S. K. Rosenthal, Radar observations of meteor winds above Illinois, Thermospheric circulation, *Willis L. Webb, ed., Mass. Institute of technology*, 205-248, 1972.

[25] Fleming, E. L., S. Chandra, M. R. Schoeberl, and J. J. Bernett, Monthly mean global climatology of temperature, wind, geopotential height and pressure from 0-120 km, *NASA Tech. Memo. 100697*, 85 pp., 1988.

[26] Hawkins, G. S., Meteors, comets, and meteorites, *McGraw-Hill*, New York, U.S.A., 1964.

[27] Hocking, W. K., T. Thayaparan, and J. Jones, Meteor decay times and their use in determining a diagnostic mesospheric temperature-pressure parameter: methodology and one year of data, *Geophys. Res. Lett.*, 23, 2977-2980, 1997.

[28] Hughes, D. W., Cosmic dust, *Willey*, Chichester, 1978.

[29] Jenniskens, P., Meteor stream activity II. Meteor outbursts, *Astron. Astrophys.*, 295, 206-235, 1995.

[30] Jones, J., On the decay of underdense radio meteor echoes, *Mon. Not. R. Astr. Soc.*, 173, 637-646, 1975.

[31] Jones, J., The decay of radio echoes from meteors with particular reference to their use in the determination of temperature fluctuations near the mesopause, *Ann. Geophysicae*, 13, 1104-1106, 1995.

[32] Jones, J., B. A. McIntosh, M. Scmek, Ozone and the duration of overdense radio meteors, *J. Atmos. Terr. Phys.*, 52, 253-258, 1990.

[33] Jones, J. and J. Jones, Ionic diffusion in meteor trails, *J. Atmos. Terr. Phys*, 52, 185-191, 1990.

[34] Jones, J., and P. Brown, The radiant distribution of sporadic meteors, *Planet. Space Sci.*, 42, 123-126, 1994.

[35] Jones, W., Theory of diffusion of meteor trains in the geomagnetic field, *Planet. Space Sci.*, 39, 1283-1288, 1991.

[36] Kaiser, T. R., Radio echo studies of meteor ionization, *Adv. Phys. (Phil. Mag. Supp.,)* 2, 495-544, 1953.

[37] Kaiser, T. R., W. M. Pickering, and C. D. Watkins, Ambipolar diffusion and motion of ion clouds in the earth's magnetic field, *Planet. Space Sci.*, 17, 519-552, 1969.

[38] Lovell, A. C. B., Meteor astronomy, *Oxford University Press*, London, U.K., 1954.

[39] Manning, L. A. O., O. G. Villard, and A. M. Peterson, Meteoric echo study of upper atmospheric winds, Proc. *Inst. Radio. Engrs.*, 38, 877-883, 1953.

[40] Manning, L. A. O., The initial radius of meteoric ionization, *J. Geophys. Res.*, 63, 81-196, 1958.

[41] Mawrey, R. S., and A. D. Broadhurst, Comparison of predicted and measured detection rates of meteor signals, *Radio Sci.*, 28, 415-427, 1993.

[42] McDaniel, E. W., and E. A. Mason, Mobility and diffusion of ions in gases, *John Willey*, New York, 1973.

[43] McDonnell, J. A. M., N. McBride, and D. J. Gardner, The leonid meteoroid stream: spacecraft interactions and effects, *University of Kent*, U.K., 1997.

[44] McIntosh, B. A., The effect of wind shear on the decay constant of meteor echoes, *Can. J. Phys.*, 47, 1337-1341, 1969.

[45] McKinley, D. W. R., and P. M. Millman, A phenomenological theory of radar echoes from meteors, *Proc. Inst. Radio Engrs.*, 37, 364-375, 1949.

[46] McKinley, D. W. R., Meteor science and engineering, *McGraw-Hill*, New York, 1961.

[47] Namboothiri, S. P., A. H. Manson, and C. E. Meek, E region real heights and their implications for MF radar derived wind and tidal climatologies, *Radio Sci.*, 28, 187-202, 1993.

[48] Newton, H. A., The original accounts of the displays in former times of the November star-showers, *Am. J. Sci.*, 37, 377-389, 1864.

[49] Olsson-Steel, D., and W. G. Elford, The height distribution of radio meteors: observations at 2 MHz, *J. Atmos. Terr. Phys.*, 49, 243-258, 1987.

[50] Phillips, E., Wind structure from the amplitude fluctuations in persistent radio meteor echoes, *Planet. Space Sci.*, 17, 553-559, 1969.

[51] Poulder, E. M., and W. J. Baggaley, Radiowave scattering from meteor in ionization, *J. Atmos. Terr. Phys.*, 39, 757-768, 1977.

[52] Poulder, E. M., and W. J. Baggaley, The application of radio-wave scattering theory to radio-meteor observations, *Planet. Space sci.*, 26, 969-977, 1978.

[53] Reddi, C. R., K. Rajeev, and R. Ramkumar, Annual and semiannual temperature oscillations at the mesopause levels over Trivandrum (8.5° N, 78° E), *J. Geophys. Res.*, D5, 8925-8931, 1993.

[54] Sander, K. F. and G. A. L. Reed, Transmission and propagation of electromagnetic waves, *Cambridge university press,* New York, U.S.A., 1986.

[55] Sato, T., Radar principles, *Handbook for MAP,* 19-53, 30, 1989.

[56] Skolnik, M., Radar handbook, *McGraw-Hill publishing company,* Toronto, Canada, 1990.

[57] Steel, D. I., and W. G. Elford, The height distribution of radio meteors: comparison of observations at different frequencies on the basis of standard echo theory, *J. Atmos. Terr. Phys.,* 53, 409-417, 1991.

[58] Stohl, J., Seasonal variation in the radiant distribution of meteors, Physics and dynamics of meteors, *Physics and dynamics of meteors (edited by L. Kresak and P. M. Millman),* Reidel, Dordrecht, 298-303, 1968.

[59] Tetenbaum, D., S. K. Avery, and A. C. Riddle, Observations of mean winds and tides in the upper mesosphere during 1980-1984, using the Poker Flat, Alaska, MST radar as a meteor radar, *J. Geophys. Res.,* 91, D13, 14539-14555, 1986.

[60] Thomas, R. M., P. S. Whitham, and W. G. Elford, Response of high frequency radar to meteor backscatter, *J. Atmos. Terr. Phys.,* 50, 703-724, 1988.

[61] Tsutsumi, M., T. Tsuda, and T. Nakamura, Temperature fluctuations near the mesopause inferred from meteor observations with the middle and upper atmosphere radar, *Radio Sci.,* 29, 599-610, 1994.

[62] Wang, S. T., D. Tetenbaum, B. B. Balsley, R. L. Obert, S. K. Avery, and J. P. Avery, A meteor echo detection and collection system for use on VHF radars, *Radio Sci.,* 23, 46-54, 1988.

[63] Whipple, F. L., Photographic meteor orbits and their distribution in space, *Astron. J.,* 59, 201-217, 1954.

[64] Yeomans, D. K., K. K. Yau, and P. R. Weissman, The impending appearance of comet Tempel-Tuttle and the Leonid meteors, *Icarus,* 124, 407-413, 1996.